Applied Catalysis B: Environmental 234 (2018) 79–89

Contents lists available at ScienceDirect

Applied Catalysis B: Environmental

journal homepage: www.elsevier.com/locate/apcatb

Control over energy level match in Keggin polyoxometallate-TiO_2 microspheres for multielectron photocatalytic reactions

Han Zheng, Changhua Wang*, Xintong Zhang*, Yingying Li, He Ma, Yichun Liu

Center for Advanced Optoelectronic Functional Materials Research, and Key Laboratory for UV-Emitting Materials and Technology of Ministry of Education, Northeast Normal University, Changchun 130024, China

ARTICLE INFO

Keywords:
Photocatalytic
Energy level match
Solar fuels
Multielectron transfer
Polyoxometallate

ABSTRACT

Recent years have witnessed that polyoxometallate (POM) is promising to mediate electron transfer on TiO_2 for enhanced photocatalysis. Therein, significant progress is made on photooxidation process, which mainly involves single electron transfer. It still represents a major challenge to develop POM-TiO_2 composites to promote multielectron transfer, such as in CO_2 reduction. In this work, we assembled oxygen-defected TiO_2-Keggin POM microspheres by ultrasonic spray pyrolysis technique for multielectron transferred reactions including mineralization of gaseous acetaldehyde and CO_2 reduction. Comprehensive analysis including transient photovoltage, surface photovoltage, and photochromic phenomena reveal that oxygen defects could induce better energy level match and hence mediate multielectron transfer. With variation of loading amount and kind of POM, the (5 wt %) $H_3PW_{12}O_{40}$ (HPW)-TiO_2 displays the highest activity among composites of HPW-TiO_2, $H_4SiW_{12}O_{40}$ (HSiW)-TiO_2, and $H_3PMo_{12}O_{40}$ (HPMo)-TiO_2, which is consistent with the best energy level match between defective TiO_2 and $H_3PW_{12}O_{40}$. The strategy of assembly of POM-TiO_2 microspheres provides a facile and promising solution to promote multielectron reaction for environmental purification and solar-to-fuel conversion.

1. Introduction

Semiconductor photocatalysis is considered as a promising technology for solar fuels generation and environmental remediation [1–3]. With the progress of photocatalytic research, it has been witnessed that photoinduced multielectron transfer is harder than single electron transfer and remains a highly relevant challenge due to the more probable recombination of charge carriers [4–6]. For example, TiO_2 works as an efficient photocatalyst on remediation of environmental organic pollutant, by which single electron transfer pathway dominates the early stages of reaction [7–9]. Nevertheless, TiO_2 and even benchmark P25 exhibit poor mineralization by which multielectron transfer pathway dominates the last stage of reaction. Also, they enable CO_2 reduction to CO via two electron transfer but not CH_4 via eight electron transfer. In this regard, further efforts are being made on promotion of multielectron transfer to make photocatalyst more efficient in solar energy conversion.

As is well reported, grafting of cocatalyst on semiconductor oxide facilitate efficient charge separation [10–13]. Unfortunately, the charge carriers in semiconductor oxide are intrinsically scattered and tend to participate in surface redox reactions via single electron transfer. Different from the scatter nature of charge carriers in semiconductor oxide, increasing research documented that introduced oxygen defects effectively trap photogenerated carriers and facilitate charge accumulation [14–20]. On grafting cocatalyst onto defective semiconductor oxide, the integration of exterior charge transfer and interior trapping is favored for onset of multi-electron transfer. In spite of this, it is critical to create an energy level match between energy level of trapping electrons and reduction potential of surface cocatalyst. For example, researchers have developed a series of strategies of combining cationic ion doping or self-doping with cocatalyst grafting [20–25]. By these strategies, doping of cationic ion or Ti^{3+} self-doping can produce energy level below the conduction band of TiO_2, which match well with the potential of multielectron reduction of O_2 over surface grafted M_xO nanocluster cocatalyst (Cu_xO, Fe_xO, etc.). Benefiting from the multielectron transfer, ultrahigh rate of CO_2 evolution via mineralization is achieved in degradation of gaseous isopropyl alcohol. Therefore, introduction of defect level in TiO_2 to meet energy level match with reduction potential of surface cocatalyst is a promising mean to facilitate multielectron transferred reaction.

Keggin type POMs have been undoubtedly recognized as electron acceptors once they meet TiO_2, due to their lower energy level of LUMO than that of conduction band of TiO_2 [26–30]. Inspired by aforementioned considerations on defective TiO_2, we anticipate that energy level

* Corresponding authors.
E-mail addresses: wangch100@nenu.edu.cn (C. Wang), xtzhang@nenu.edu.cn (X. Zhang).

https://doi.org/10.1016/j.apcatb.2018.04.015
Received 18 January 2018; Received in revised form 30 March 2018; Accepted 10 April 2018
Available online 20 April 2018

match between defective TiO_2 and POM can further extend the application of POM-TiO_2 composites from single-electron-transfer dominated oxidation for environmental remediation to that of multi-electron-transfer dominated reduction for solar fuels. More interestingly, Lv et al revealed that the POM anions interact mainly with Ti-OH_2^+ sites on the surface of TiO_2 rather than replacement of surface hydroxyl group [31]. By this way, the TiO_2 surface can be fascinatingly covered by POM without decreasing the amount of surface hydroxyl group. The preservation of surface hydroxyl group after compositing TiO_2 with POM provides a very important clue for multi-electron-transfer reaction. That is, surface hydroxyl group can be oxidized by photogenerated holes and thereafter promote the release of proton [32], multi-electron-transfer reaction can proceed more easily via proton coupled electron transfer such as oxygen reduction (e.g. $2e^-/2H^+$ to H_2O_2, $4e^-/4H^+$ to H_2O), CO_2 reduction (e.g. $2e^-/2H^+$ to CO, $8e^-/8H^+$ to CH_4) and etc.

Herein, by means of a simple ultraspray pyrolysis technique, loading of POM and introduction of oxygen vacancy in TiO_2 was achieved simultaneously and finally POM-TiO_{2-x} microspheres were produced. The kind and content of Keggin POM including HSiW, HPW and HPMo are optimized for energy level match and promotion of multielectron transfer at POM-TiO_2 interface. Model reaction including mineralization of gaseous acetaldehyde and CO_2 reduction governed by multi-electron transfer process are tested to evaluate the photocatalytic activity. The results demonstrate that the presence of oxygen vacancy is adverse to charge separation, and whereas oxygen vacancy type POM-TiO_2 become a better candidate for multielectron involved reaction due to proper energy level match induced multielectron transfer. Therein, HPW (5 wt%)-TiO_2 exhibits the highest mineralization yield and CH_4 selectivity among all samples, benefiting from best energy level match and strong interaction between TiO_2 and HPW component. This simple but effective means on the basis of energy level match can be extended to apply doped semiconductor-POM system for highly active photocatalyst as well.

2. Materials

TiO_2 powders (Degussa P25) were obtained from Nihon Aerisol Co. Keggin polyoxometallates, including $H_3PW_{12}O_{40}$, $H_4SiW_{12}O_{40}$ and $H_3PMo_{12}O_{40}$, were purchased in analytical purity from Chinese National Medicine Group Chemical Reagent Co. CH_4 (0.3 vol% in N_2) and CO (50 vol% in N_2) were obtained from Beijing AP BAIF Gases Industry Co., Ltd. All chemical reagents were used as received, without further purification.

2.1. Characterization

Morphology and composition analyses were carried out on a FEI quanta 250 field emission scanning electron microscope (FESEM) and high resolution electronic micrographs were acquired using a JEOL JEM-2100 transmission electron microscope (TEM) operated at an acceleration voltage of 200 kV. X-ray powder diffraction (XRD) patterns were recorded using a Rigaku, D/MAX-2500 X-ray diffractometer with Cu Kα radiation. The UV–visible (UV–vis) diffuse reflectance (DR) spectra of the samples were collected using a PerkinElmer UV WinLab spectrophotometer. Fourier transform infrared (FTIR) spectra were recorded using a Nicolet Magna 560 FTIR spectrometer. X-ray photoelectron spectroscopy (XPS) was performed using a VGESCALAB MKII instrument with a Mg Kα ADES source at a residual gas pressure below 10^{-8} Pa. Electron spin resonance (ESR) measurements were conducted on an X-band CW-EPR Bruker ElEXSYS spectrometer in the X band (9.38 GHz) at 90 K equipped with a cylindrical cavity operating at 100 kHz field modulation. Transient photovoltage spectroscopy (TPV) and surface photovoltage spectroscopy (SPV) measurements were carried out using a lab-made instrument according to the references [33–36]. Zeta potential was measured using a DLS Zeta potential analyzer (ZS90) from Malvern Instruments.

2.2. Preparation of TiO_2-POM composite photocatalyst

POM-TiO_2 composite microspheres were prepared using the ultrasonic spray pyrolysis method. Typically, P25 TiO_2 powder (3 g) was dispersed into 1000 ml of water with a glass beaker, and added some 0.005 M HPW aqueous solution into the beaker to form a mixed suspension. Subsequently, the suspension was atomized using an ultrasonic nebulizer, and the formed mist was passed through a quartz tube heated at 823 K. Then, powder was collected at an electrostatic collecting device connected to the end of the quartz tube. Finally, Samples of 0, 5, 10, and 20 wt% POM-loaded TiO_2 were obtained. The color of as-obtained powders changes from original white of P25 to grey or light blue, indicating that they are defective. For comparison, POM-TiO_2 composites with no defects were prepared by direct drying of the POM-TiO_2 colloid suspension at 70 °C in air and turned to no USP process. By this way, the obtained powders perfectly maintained the original white color of P25.

2.3. Photocatalytic reduction of CO_2

The photocatalytic reduction of CO_2 was carried out in a closed gas system (Beijing CEAU Light Technology Co., Ltd, China). 1.3 g $NaHCO_3$ was added at the bottom of reaction (350 mL) firstly. Then, 50 mg of the TiO_2-POM microspheres powder was uniformly dispersed in a sample holder with a geometric area of 1.23 cm^{-2}. Prior to the light irradiation, the above system was thoroughly vacuum-treated to remove the air completely, and then 5 mL 4 M H_2SO_4 was injected into the reactor to react with $NaHCO_3$ to achieve 1 atm CO_2 gas. After that, the reactor was irradiated from the top by a 150 W xenon lamp (Hayashi UV410) which emits light in the wavelength range of 350–700 nm. The light intensity used to irradiate the samples was determined to be 20 mW cm^{-2} at 365 nm using a light intensity meter from Beijing Normal University. During the irradiation, 1 mL of gas was taken from the reaction cell for subsequent qualitative analysis by gas chromatograph (GC2014, SHIMADZU Co.), equipped with a Shin-carbon ST column and a flame ionization detector. The quantification of the production yield was based on a calibration curve. The outlet gases was determined to be CO, CH_4 and CO_2.

3. Results and discussion

3.1. USP procedure based on isoelectric point of POM-TiO_2 suspension

As reported in previous study, USP can be served as a facile and scalable methodology to fabricate porous microspheres [37–40]. Three sequential stages are involved: (1) formation of precursor droplets by the ultrasonic nebulization of a colloid solution; (2) transport of droplets flux across the heating furnace by inert gas, accompanied by solvent evaporation and pyrolysis of precursor; (3) self-assembly and aggregation of nanoparticles into porous microspheres by further annealing. Up until now, we have successfully fabricated porous microspheres by employing TiO_2 nanoparticles [41], Nb doped TiO_2 nanoparticles [42], WO_3 nanosheets and Pt nanoparticles as building blocks [43]. In this work, P25 TiO_2 nanoparticles suspended in deionized water at a 3 g L^{-1} concentration formed a relatively stable dispersion with a zeta potential of 21.5 mV (as shown in Fig. 1), which facilitates generation of uniform precursor droplets for ultrasonic sprayed pyrolysis. Upon addition of POM into TiO_2 colloid solution, the value of zeta potential is drastically decreased and value of zero is close to isoelectric point when the weight percentage of POM is about 5 wt%, which indicates strong interaction between protonated TiO_2 and POM anion. With further increase of POM content, the zeta potential is reversed from positive to negative and become stable until the loading content is higher than 20%. It indicates that the stability of P25 colloid is deteriorated once it meets POM solution. However, the as-formed particles aggregates can be re-dispersed with the increase of POM

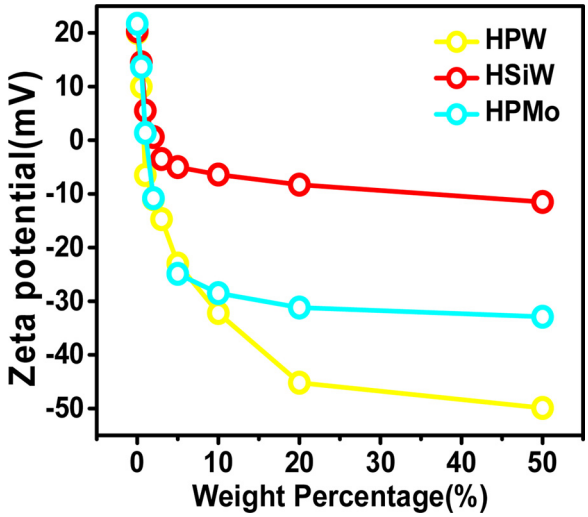

Fig. 1. Variation of zeta potential of POM-TiO_2 colloid suspension with the increase of POM weight percentage.

content and a stable colloid solution is re-formed. In this regard, the weight ratio of POM in POM-TiO_2 composites is selected as 5%, 10% and 20%, respectively, to ensure fabrication of uniform microspheres by USP process from colloid solution.

3.2. Morphology of POM-TiO_2 composites and high dispersion of POM on TiO_2

Fig. 2a–c show the typical SEM images of as-sprayed HPW-TiO_2 composites. As can be seen, the original morphology of nanoparticles aggregates is disappeared. Instead, microspheres with diameters in the range of 2–5 μm are produced after USP process. Moreover, no morphology difference is observed between HPW-TiO_2 composites with different POM content. Meanwhile, other HSiW-TiO_2 and HPMo-TiO_2 composites are composed of microspheres and there is also no obvious morphology difference in comparison with that of HPW-TiO_2 composite (not shown). TEM images in Fig. 2d–f confirm the microsphere structure of above typical HPW-TiO_2 samples. Meanwhile, EDS mapping was carried out to investigate the distribution of POM on the surface of TiO_2 nanoparticles (Fig. 2d–f, inset). In all cases, a homogeneous distribution of P and W element is clearly observed in microspheres. On closer observation, similar pattern between Ti, P and W elements is confirmed. Additionally, XRD is employed to further study the crystal phase of HPW-TiO_2. As shown in Fig. S1, even though the loading amount of POM is as high as 20 wt%, no additional diffraction peaks attributed to POM or decomposed POM are detected in all samples, confirming the high dispersion of POM on the surface of TiO_2. Moreover, the relative intensity ratio of diffraction peaks corresponding to anatase and rutile phase remain unchanged, indicating the introduction of POM has no influence on the crystal phase of P25. Accordingly, it is suggested that POM is highly dispersed on the surface of TiO_2 nanoparticles, which is beneficial to efficient charge carrier separation in photocatalysis.

FT-IR spectra are employed to understand the chemical state of POM on TiO_2 microspheres surface. In Fig. 3a–c, the intensity of the W—O bands at 700–1200 cm^{-1} is observed and proportional to the amount of POM on TiO_2 [44]. Notably, these bands are too weak to be detected in POM-TiO_2 microspheres with a considerable loading amount of 5% because of a high dispersion of POM on TiO_2 by USP process, which is in agreement with above TEM and EDS results. A single peak of Si—O at 1020 cm^{-1} for HSiW, P—O at 1080 cm^{-1} for HPW and P—O at 1060 cm^{-1} for HPMo [45,46], respectively, is consistently remained in composites with loading content higher than 5 wt %, indicating that POM structure are essentially preserved in POM-TiO_2 microspheres composites. Diffused reflectance spectra is further investigated to study the structure of POM-TiO_2 composites, which is shown in Fig. 3d–f. In general, all samples exhibit similar absorption band at wavelengths below 420 nm, which is mainly attributed to the electron transition from O2p to Ti3d orbital in TiO_2. We note that the absorption curve of P25-USP in the region of 325–405 nm is not as steep as that of fresh P25 (Fig. 3d, inset), indicating an introduction of defects

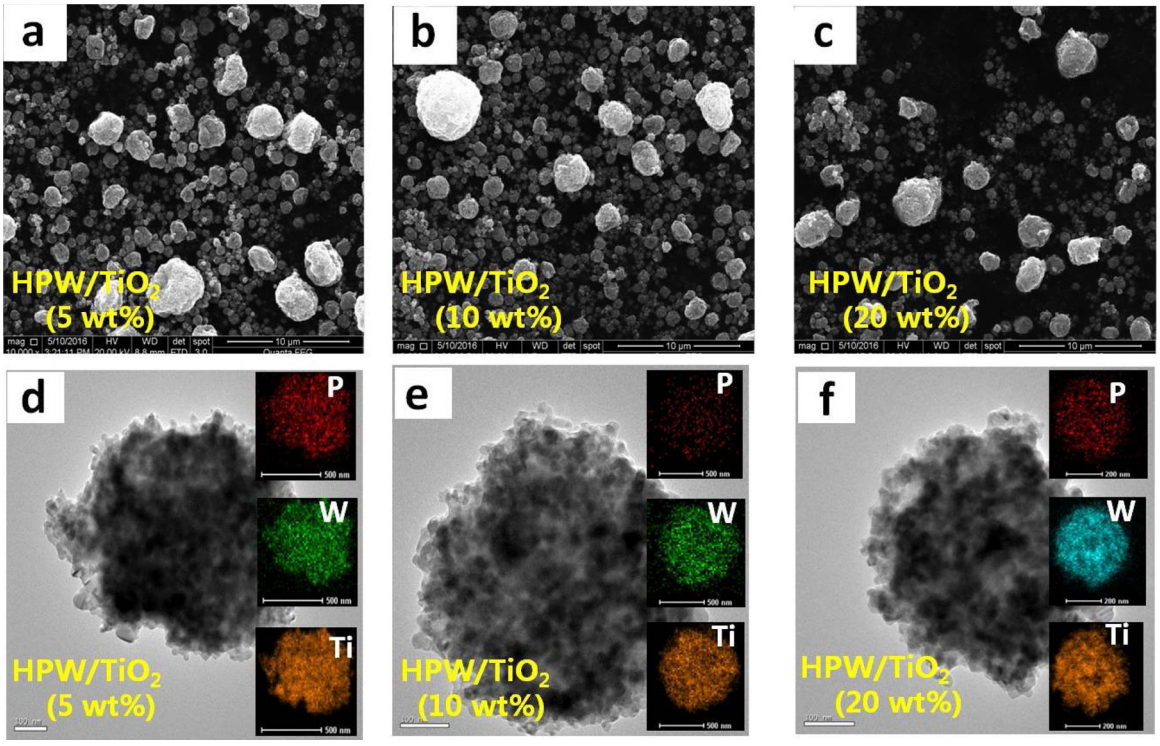

Fig. 2. SEM, TEM images and EDS mappings of HPW-TiO_2 composites: (a,d) HPW(5 wt%)-TiO_2; (b,e) HPW(10 wt%)-TiO_2; (c,f) HPW(20 wt%)-TiO_2.

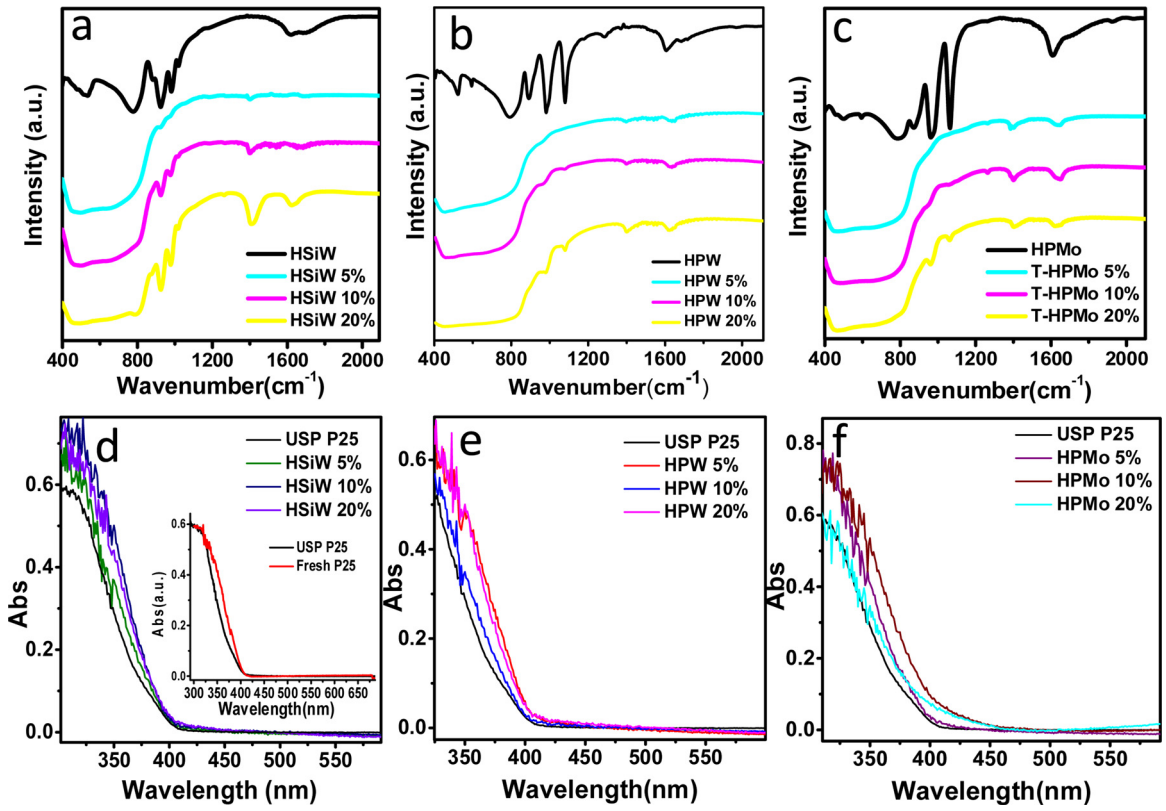

Fig. 3. (a–c) FT-IR spectra of pure POM and different POM-TiO_2 composites; (d–f) UV–vis spectra of TiO_2 and different POM-TiO_2 composites.

in P25 microspheres after USP process. The absorbance bands at ca. 250 nm being assigned to charge transfer from O_{2p} to W_{5d} in the Keggin unit are not detected in all microspheres composites [46], which is due to the ultra-small size of POM cluster and their high dispersity on TiO_2 surface. In addition to main UV absorption, absorption range in some samples can be slightly extended to visible region and the visible absorption increases with the increase of POM content. This is consistent with the light blue color of HPMo-TiO_2 samples and gray color of other samples. On comparing different kinds of POM, order of the increment of visible light absorption is HPMo > HPW ~ HSiW. As is reported, the thermal stability of Keggin POM is HPW > HSiW > HPMo [47]. When recalling the USP process, POM-TiO_2 droplets pass through the furnace and then subject to rapid heat treatment at 550 °C, possibly inducing a slight reduction of POM. Owing to its lowest thermal stability, HPMo may undergo a weak thermal reduction and thus HPMo-TiO_2 composites exhibit observable visible-light absorption.

The surface structural information of TiO_2-POM composites are further determined by X-ray photoelectron spectrometry. Fig. 4a and b show the XPS spectra of Ti2p and O1s spectra of fresh P25, USP-P25, and HPW-TiO_2 composites. By comparing the binding energy of Ti2p and O1s peaks of fresh P25 and USP-P25, an obvious positive shift is occurred after assembly of P25 nanoparticles by USP, which is previously observed in the case of oxygen vacancy typed TiO_2 as well [48]. As for the HPW-TiO_2 composite, the binding energy of Ti2p and O1s peaks further increase at loading amount of 5 wt%, and whereas gradually fall at loading amount of 10 wt% and 20 wt%. The shift to higher binding energy of Ti2p and O1s peaks in HPW-TiO_2 can be resulted from the formation of W—O—Ti bond. That is, since the electronegativity of W^{6+} (1.70) is higher than Ti^{4+}(1.54), the formation of W—O—Ti bond will reduce the electron density around Ti^{4+} and hence leads to higher binding energy of Ti2p peak. Moreover, this shift can be more significant when HPW is ultradispersed on TiO_2, where strong interaction between HPW and TiO_2 exisits. The largest degree of positive shift of binding energy of Ti2p and O1s peaks in (5 wt%) HPW-TiO_2

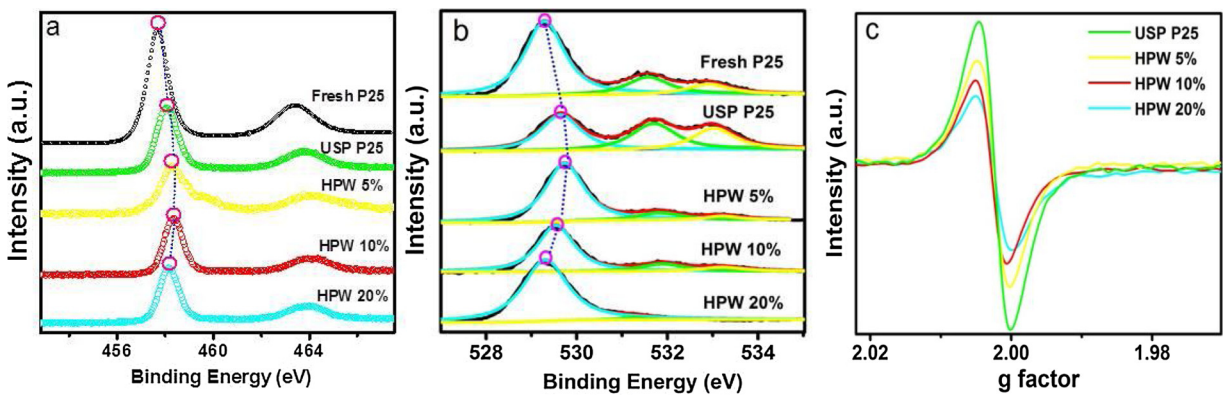

Fig. 4. (a) Ti2p XPS spectra, (b) O1s XPS spectra of TiO_2 and (c) ESR spectra of TiO_2 and HPW-TiO_2 composites.

can be ascribed to the strongest interaction between TiO_2 and HPW, which has been indicated by the most significant variation of zeta potential of (5 wt%) POM-TiO_2 suspension before USP preparation. However, with further increase of HPW loading, HPW component tend to aggregate and weaken its interaction with that of TiO_2. Thus, the degree of shift of binding energy of Ti2p and O1s tends to decrease at loading amount higher than 5 wt%. To further confirm the introduction of oxygen vacancy by USP technique, ESR spectra is collected and the results are shown in Fig. 4c. For all samples, a signal is observed at g = 2.003, which is related to the interaction of surface oxygen vacancy sites with adsorbed atmospheric O_2. This is consistent with reported results [49,50] and our previous works [48] on oxygen vacancy typed TiO_2, confirming the existence of oxygen vacancy in as-obtained samples. For USP P25, a significant signal appeared at g = 2.003, demonstrating USP technique could bring oxygen vacancy into TiO_2. In addition, from the intensity of the signals over different HPW-TiO_2 composites, we can speculate that the oxygen vacancy can be partly covered but still preserved when the loading amount of HPW reaches 20%.

3.3. Studies on charge transfer and separation at POM-TiO_2 interface by TPV and SPV

TPV techniques provide direct information on the generation, separation, and recombination of photogenerated charge carriers [33–36]. At shorter time scale (10^{-8}–10^{-6} s), the photovoltage response means charge separation induced by drift process in space-charge regions and featured by the first peak (named Peak 1). As shown in Fig. 5a–c, positive photovoltage signals are produced with the laser pulse and increased dramatically to maximum value, which is in agreement with the charge separation in the space-charge regions of n-type semiconductor [51]. That is, in bulk n-type TiO_2, the band bending is upward, build-in electric field will make photogenerated electrons drift to bulk and holes drift to surface. Note that there is no significant difference in the time of Peak 1 between all samples, indicating similar mobility of carriers in the space-charge region.

At mediate time scale (10^{-6}–10^{-4} s), the photovoltage response means charge separation induced by diffusion process of charge carriers and featured by a second peak (named Peak 2). As shown in Fig. 5a–c, the photovoltage response significantly varies from sample to sample. Firstly, Peak 2 does not appear over USP TiO_2 (Fig. 5a, inset), indicating that the defects in terms of oxygen vacancies most probably act as recombination centre. Secondly, the positive signals can be lasted until Peak 2 appears over all TiO_2-POM composites. Moreover, time at Peak 2 changes with the kind and loading percentage of POM in TiO_2-POM composites, which is listed in Table 1. Accordingly, the order of time at Peak 2 is summarized as following:

(1) HPW (5%)-TiO_2 > HPMo (5%)-TiO_2 > HSiW (5%)-TiO_2 > fresh TiO_2 > USP TiO_2
(2) HPW (5%)-TiO_2 > HPW (20%)-TiO_2 > HPW (10%)-TiO_2 > fresh TiO_2 > USP TiO_2
(3) HSiW (5%)-TiO_2 > HSiW (20%)-TiO_2 > HSiW (10%)-TiO_2 > fresh TiO_2 > USP TiO_2
(4) HPMo (20%)-TiO_2 > HPMo (5%)-TiO_2 > HPMo (10%)-TiO_2 > fresh TiO_2 > USP TiO_2

Since the TPV response at this time scale corresponded to the diffusion process of charge carriers, longer time of Peak 2 indicates that the photoinduced charges have longer time to participate in the photocatalytic reaction before recombination. Accordingly, the absence of Peak 2 in the TPV spectra of USP P25 means poorer performance in charge separation than that of fresh P25, which is believed to be induced by the introduction of defects of oxygen vacancy in P25. For order (1), it means that the HPW-TiO_2 composite shows an obvious retardation of Peak 2 in comparison with other POM-TiO_2, indicating a longer carrier lifetime and lower recombination rate of electron-hole pairs. As for order (2) and (3), they consistently reflect a better charge separation with 5% loading than that of 10% and 20% loading over HPW-TiO_2 or HSiW-TiO_2. Differently, for HPMo-TiO_2 composites, HPMo (20%)-TiO_2 takes the longest time for Peak 2 among all samples, which is related to part decomposition of HPMo and will be discussed

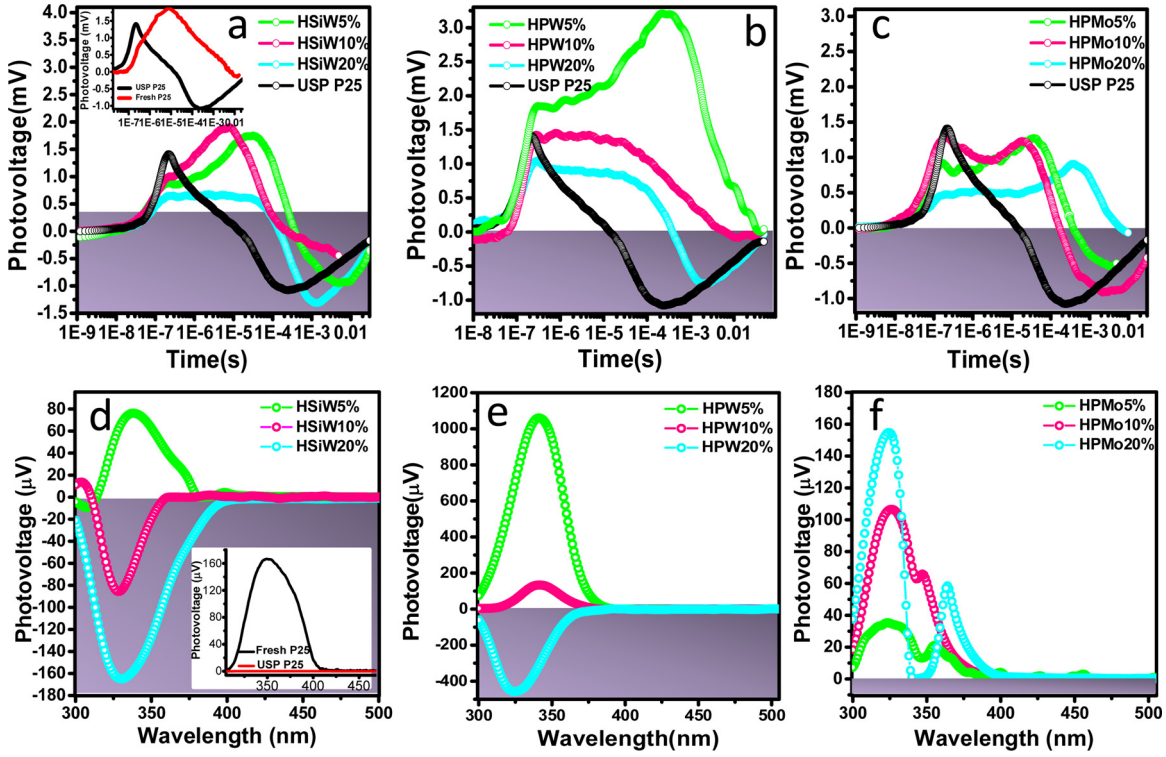

Fig. 5. (a–c) TPV spectra of TiO_2 and different POM-TiO_2 composites; (d–f) SPV spectra of TiO_2 and different POM-TiO_2 composites.

Table 1
Analysis results from TPV spectra of different samples.

Results	Sample										
	P25 Fresh	P25 USP	HsiW 5%	HsiW 10%	HsiW 20%	HPW 5%	HPW 10%	HPW 20%	HPMo 5%	HPMo 10%	HPMo 20%
Peak 1 Time (10^{-7} s)	3.09	2.24	2.28	2.37	2.39	**3.09**	2.76	2.78	1.68	2.19	1.78
Peak 2 Time (10^{-5} s)	0.77	**No**	3.10	0.76	2.90	**29**	3.13	3.84	3.83	1.84	**42.47**
Turning Point Time (10^{-4} s)	61.85	1.42	4.02	2.50	1.47	**383.74**	45.55	3.71	3.94	1.60	**63.69**

The bold value represents the most important information in the table.

later.

At longer time scale (10^{-4}–10^{-2} s), all samples display a more striking feature of TPV responses in that the signal is reversed from positive photovoltage at mediate time scales to negative photovoltage at longer time scales. The time of signal reverse over different samples is listed in Table 1. Accordingly, the following information is obtained:

(1) USP TiO_2 exhibits shorter time of signal reverse than that of fresh TiO_2.
(2) TiO_2-POM composites exhibit longer time of signal reverse than that of fresh TiO_2 and USP TiO_2.
(3) HPW(5%)-TiO_2 possesses the largest time scale for signal reverse among all samples.
(4) With the increase of POM loading, time of signal reverse becomes shorter over TiO_2-HPW and TiO_2-HSiW, and whereas signal reverse time becomes abnormally longer over TiO_2-HPMo.

The photovoltage response at this stage mainly means competition between diffusion and recombination of photogenerated electrons and holes in the TiO_2-POM composites. At the turning point, the zero value of photovoltage indicates that the charge recombination rate equals to that of charge separation. Before the turning point, the positive signals indicate that photogenerated holes are aggregated on the surface, which is due to the higher mobility of electrons from surface to bulk and POM as trapping cites for electrons in TiO_2. After the turning point, the negative signals indicate that photogenerated electrons are aggregated on the surface, which is deemed to be related to back transfer of electrons from reduced POM to TiO_2. On recalling the time order of turning point for TiO_2-POM composites, the results can be correspondingly explained as following:

(1) The defects of oxygen vacancy in USP TiO_2 accelerate charge recombination.
(2) The photogenerated electrons in TiO_2 can be transferred to POM, the charge recombination can be inhibited and hence the time of turning point can be retarded in comparison with that of pristine TiO_2.
(3) For HPW-TiO_2, the electron transfer rate from TiO_2 to HPW is superior to other two interfaces between POM and TiO_2, and thus the longest time of turning point is in agreement with the best ability of charge separation across HPW-TiO_2 interface.
(4) The electron transfer from TiO_2 to POM competes with that of back transfer of electrons from POM to TiO_2, store of electrons in POM as well as electron transfer to oxygen, time difference of turning point is a synergistic effect of above processes. For HPW-TiO_2 and HSiW-TiO_2, it is believed that energy level match ensures a possible one-way flow of electron from TiO_2 to HPW and then to absorbed oxygen. However, with the increase of POM loading from 5% to 20%, coverage of POM on oxygen defects in TiO_2 should not be neglected, which may decrease the degree of energy level match and thereafter charge separation. Therefore, time of signal reverse over 10% POM-TiO_2 and 20% HSiW-TiO_2 is shorter than that of 5% POM-TiO_2. Besides, the LUMO level of POM determines its ability of oxygen reduction by electrons. For HPMo, the low position of LUMO level means difficult transfer of electron to oxygen. Alternatively, HPMo tends to store electron and partly change to heteropolyblue. In this regard, the longest time of signal reverse over 20% HPMo-TiO_2 among all HPMo-TiO_2 composites is related with the role of HPMo as electron store.

In contrast to TPV, SPV is a technique to investigate the charge transfer processes at the macro-level rather micro-level [52,53]. Thus, SPV technique is supplementally investigated to further address above kinetic behaviors of charge transfer, separation and recombination, and the results are shown in Fig. 5d–f. The obtained data are listed and understood as following:

(1) The photovoltage signal of USP TiO_2 (Fig. 5d, inset) is too low to be observed in comparison with that of fresh P25 and POM-TiO_2 composites, again confirming that oxygen defects are not good for charge separation.
(2) For all POM-TiO_2 composites, peak positions shift to shorter wavelength (blue-shift) with the increase of POM loading. The blue shift is believed to be related with the decrease of oxygen defects in TiO_2 after compositing with POM. That is, POM loading could partly heal defects in TiO_2 and thereby reduce probability of electron transition from valence band to defect-induced energy level below the conduction band.
(3) For HSiW-TiO_2 composites, photovoltage response turns negative when loading of HSiW exceeds 5%. For HPW-TiO_2 composites, 5% HPW-TiO_2 exhibits champion response of positive photovoltage among all POM composites and turns negative until the loading of HPW reaches 20 wt%. For HPMo-TiO_2 composites, they are different from HSiW-TiO_2 and HPW-TiO_2 composites in that photovoltage response does not turns negative irrespective of the increase of loading amount from 5% to 20%. These results are understood as following:

In principle, whether positive or negative photovoltage response occurs depends on charge separation ability. The stronger the positive photovoltage exhibits, the better charge separation means [33,52,53]. Accordingly, the champion response of positive photovoltage over 5% HPW-TiO_2 proves its best performance in charge separation, which is in consistent with above TPV results. The photovoltage tends to be reversed from positive to negative with the increase of POM content in HPW-TiO_2 and HSiW-TiO_2, suggesting that back transfer of electron from POM to TiO_2 compete with that of electron transfer from TiO_2 to POM and become dominant at higher POM content. Moreover, such back electron transfer is also determined by position of LUMO level of POM. As is widely reported, the reduction potential of POM depends on the electron negativity of central heteroatom (eg. P, Si) and polyatom (eg. W, Mo) [54,55]. On one hand, the reduction potential of Keggin POM decreases with increasing electron negativity of the polyatom. For example, the electron negativity of W and Mo is 2.36 and 2.16, respectively, the reduction potential of HPW is lower than HPMo. On the other hand, the reduction potential of Keggin POM decreases with decreasing electron negativity of the heteroatom. For example, the electron negativity of P and Si is 2.19 and 1.90, respectively, the reduction potential of HSiW is lower than HPW. From perspective of energy level match, back transfer of electron from HSiW to TiO_2 is

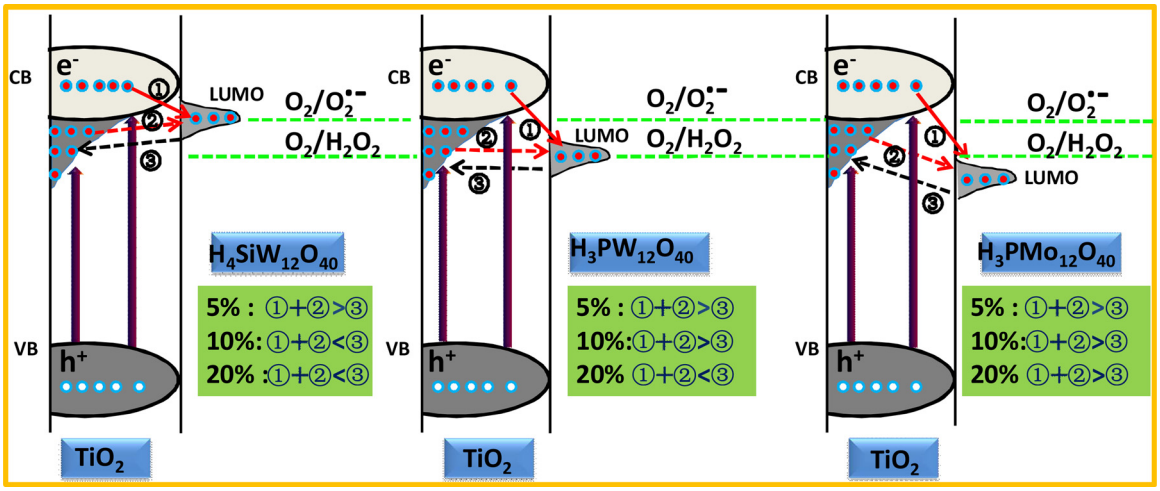

Scheme 1. Illustration of charge transfer and separation at different POM-TiO_2 interface. The signal " > " and " < " means a higher and lower probability of combined process of 1 and 2 than that of process 3, respectively.

thermodynamically more probable than HPW. As such, HSiW-TiO_2 reverse the photovoltage to negative with less content (5%) than that of HPW(20%). Since the LUMO level of HPMo is lower than that of HPW and HSiW, back transfer of electron from HPMo to TiO_2 becomes more difficult and exerts neglect influence on the charge transfer.

In combination with above results in TPV and SPS, the charge transfer at TiO_2-POM interface is illustrated in Scheme 1. The conduction band of TiO_2 locates at −0.5 eV, while LUMO level of POM for HSiW, HPW and HPMo locate at 0.06, 0.22 and 0.65 eV, respectively. Accordingly, the photogenerated electrons on conduction band of TiO_2 can be transferred to POM, which is named process ①. Meanwhile, the localized electrons by oxygen defects below the conduction band can also transfer from TiO_2 to POM, which is named process ②. Besides, the accumulated electrons in POM probably back transfer to TiO_2, which is named process ③. The presence of oxygen vacancy can decrease mismatch of energy level at TiO_2-POM interface. Specifically, the energy level of oxygen vacancy is of 0.7 eV below conduction band, energy level mismatch between TiO_2 and POM can be decreased from 0.56, 0.72 and 1.15 eV to 0.14, 0.02 and 0.45 eV for HSiW-TiO_2, HPW-TiO_2 and HPMo-TiO_2, respectively. The better energy level match between TiO_2 and POM indicates better charge separation and thereafter multielectron transfer. For oxygen vacancy typed HPW-TiO_2, it is of the best energy level match and thereby shows champion response of positive photovoltage among TiO_2-POM composites. The competition of combined process ① and ② with process ③ determines whether positive or negative response of photovoltage. When process ① and ② is dominant, a positive SPS response is produced, and whereas, when process ③ become dominant, a negative response is observed. According to the LUMO level of POM, the probability of electron back-transfer to TiO_2 is in the order: HSiW-TiO_2 > HPW-TiO_2 > HPMo-TiO_2. Therefore, in any case, the HPMo-TiO_2 composite displays a positive SPS response, indicating that electron back-transfer is difficult and processes of ① and ② are always dominant at the interface. In general, processes of ① and ② are beneficial to charge separation and thereby activity enhancement, and whereas process ③ inhibits the charge separation and has an adverse effect on activity. Hence, differences in the competition of process ① and ② with ③ will synergistically influences the charge separation, in particular, via multielectron transfer pathway.

3.4. Photocatalytic activities of POM-TiO_2 composites

The photocatalytic activity of all TiO_2-POM composites are evaluated by two typical reactions, including mineralization of gaseous acetaldehyde and CO_2 photoreduction, which depend on 8 electrons transfer and 2–8 electrons transfer, respectively. For a clear evaluation of the role of oxygen vacancy on the activity enhancement, a typical HPW(5%)-TiO_2 sample is also prepared by traditional impregnation method instead of USP technique, because the introduction of oxygen vacancy can be greatly avoided during impregnation of POM onto TiO_2.

Fig. 6 and Table 2 show the results of acetaldehyde mineralization over different samples. As can be seen, POM-TiO_2 composites except for HPMo-TiO_2 exhibit much higher photoactivities for acetaldehyde degradation than that of fresh P25 and USP TiO_2, indicating the charge transfer at POM-TiO_2 interface is beneficial to activity enhancement. In addition, HPW-TiO_2 prepared by USP method exhibits expected higher activity than that of impregnation method, indicating oxygen vacancy indeed play a key role in further enhancement of activity. In particular, there is a significantly higher removal percentage of acetaldehyde over oxygen vacancy typed HPW(5%)-TiO_2 and HPW(20%)-TiO_2 among all samples. However, on further comparison via mineralization yield, oxygen vacancy typed HPW(20%)-TiO_2 gives an inferior performance to that of HPW(5%)-TiO_2. On recalling aforementioned TPV and SPS results, oxygen vacancy typed HPW(5%)-TiO_2 exhibits better ability for charge transfer than that of HPW(20%)-TiO_2. Therefore, it is believed that the better performance of oxygen vacancy typed HPW(5%)-TiO_2 is related to a better ability of charge separation on oxygen vacancy typed HPW(5%)-TiO_2. The recycle experiments reveal that HPW(5%)-TiO_2 shows slight decrease of photocatalytic activity for degradation of acetaldehyde after five recycles (Fig. S2). Furthermore, ESR spectrum of oxygen vacancy typed HPW(5%)-TiO_2 after five runs maintains the signal of oxygen vacancy at g = 2.003 (Fig. S3), which indicates oxygen vacancy typed HPW(5%)-TiO_2 has a good stability. Since mineralization of acetaldehyde depends on multi-electron reduction of oxygen and truly demonstrates the efficiency of multi-electron transfer to oxygen, it is assumed that oxygen vacancy typed HPW(5%)-TiO_2 is particularly beneficial to charge separation and further onset of multielectron reduction of oxygen. On the contrary, reduction of oxygen over oxygen vacancy typed HPW(20%)-TiO_2 has to depend on a competition between single electron transfer to oxygen and multi-electron transfer. As such, more intermediates such as acetic acid are accumulated on the surface of oxygen vacancy typed HPW(20%)-TiO_2 catalyst and hinder the complete mineralization of acetaldehyde to CO_2. Similar to oxygen vacancy typed HPW-TiO_2 composite, the activities of oxygen vacancy typed HSiW-TiO_2 and HPMo-TiO_2 consistently decrease with the increase of POM loading, which agrees with the tendency in above photovoltage response. To understand the multi-electron transfer process during photocatalytic degradation of acetaldehyde, we tentatively monitor the intermediate product of H_2O_2 from two-electron reduction

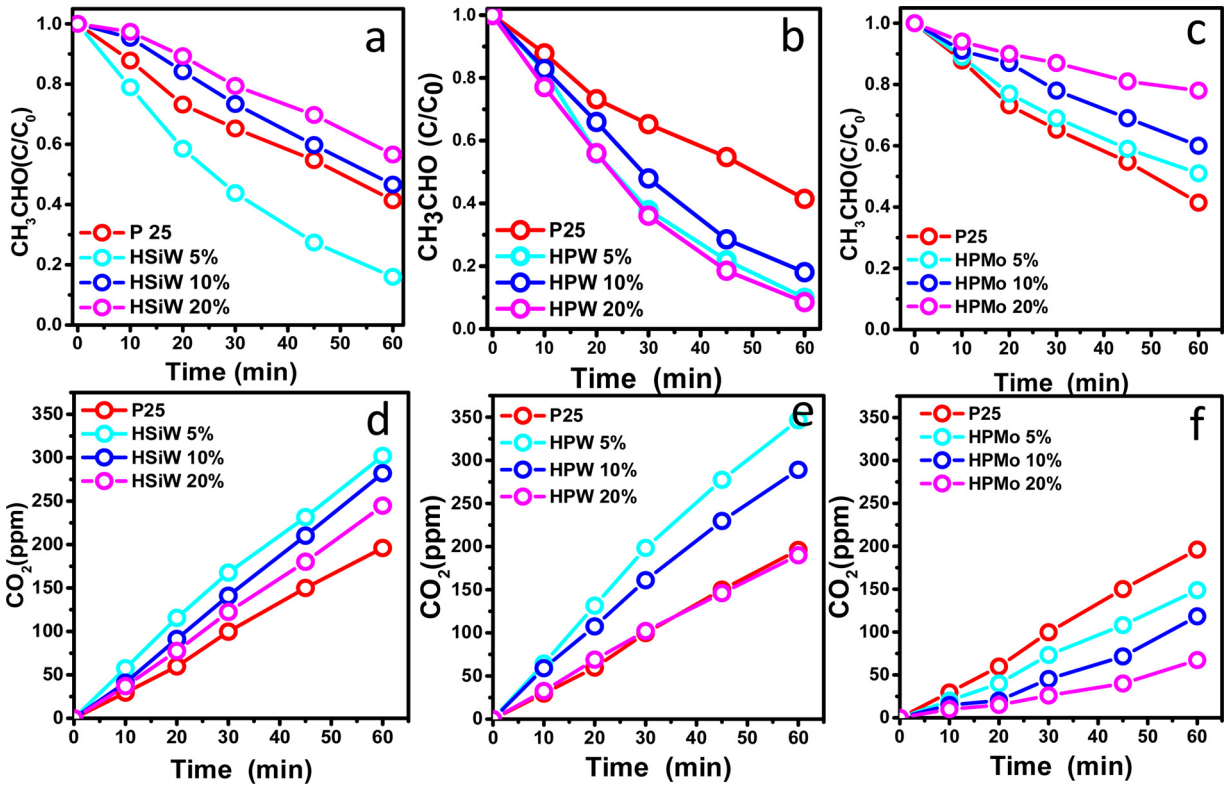

Fig. 6. Curves of acetaldehyde degradation and CO_2 evolution over different samples.

of oxygen at the gas/solid interface. The amount of H_2O_2 was determined by the DPD method [32], which is described in the supporting information in detail. In fact, previous studies have performed comparative studies on the generation of H_2O_2 over TiO_2 and HPW. Pristine HPW are known less active for H_2O_2 production than that of pristine TiO_2 because of back reaction between reduced HPW and H_2O_2. For example, Chen et al. [56] observed a sharp decrease of H_2O_2 amount when HPW was added into TiO_2 suspension during UV irradiation. Herein, we also hardly detect the production of H_2O_2 over HPW(20%)/TiO_2 (Fig. S4), which is consistent with reported inhibition effect of HPW on H_2O_2 production. However, as for HPW (5%)/TiO_2, it interestingly displays a stronger absorption of DPD/POD-H_2O_2 solution than that of USP P25, as shown in Fig. S4. This demonstrates that loading HPW of 5% increases the production amount of H_2O_2 over USP TiO_2. On ruling out the possibility of promoting generation of H_2O_2 by single HPW component, it is believed that higher amount of H_2O_2 over HPW (5%)/TiO_2 than USP P25 indeed originates from double-electron-transfer, which is induced by the energy-level-match between oxygen vacancy and LUMO level of HPW.

The results of photocatalytic test via CO_2 reduction over POM-TiO_2 composites are shown in Figs. 7 and S5. Control experiments indicated that no CO and CH_4 were detected in the absence of photocatalyst or light. Moreover, without introduction of CO_2, the photocatalyst under UV light irradiation showed no CO_2 reduction products. Therefore, CO_2 was the sole carbon source of CO_2 reduction products. Generally, in the gas-solid photocatalytic reaction system, CH_4 and CO are the main reduction products. However, CO was the sole product over oxygen vacancy typed P25. Interestingly, after compositing with POM, not only CO but also CH_4 are produced as main products.

In detail, for the generation of CO, the production rate are in order: HPW(10%)-TiO_2 > HPW(5%)-TiO_2 > HSiW(5%)-TiO_2 > HPMo (5%)-TiO_2 ~ fresh P25 > USP P25. For the generation of CH_4, the production rate are in order: HPW(5%)-TiO_2 > HPW(10%)-TiO_2 > HSiW(5%)-TiO_2 > HPMo(5%)-TiO_2 ~ fresh P25 > USP P25. Accordingly, HPW(5%)-TiO_2 and HPW(10%)-TiO_2 are more active than other composites. On further comparing activity between HPW(5%)-TiO_2 and HPW(10%)-TiO_2, HPW(5%)-TiO_2 displays a lower generation rate of CO but a higher generation rate of CH_4 than that of HPW(10%)-TiO_2, respectively. Because production of CO and CH_4 from CO_2 and H_2O proceed via transfer of two and eight electrons, as shown in the following equation:

$$CO_2 + 2\,e^- + 2\,H^+ = CO + H_2O\ E_1 = -0.53\,V$$

$$CO_2 + 8\,e^- + 8\,H^+ = CH_4 + 2\,H_2O\ E_2 = -0.24\,V,$$

Table 2
Photocatalytic results including removal ratio of acetaldehyde and mineralization over different samples.

Results	Sample										
	P25 USP	HsiW 5% USP	HsiW 10% USP	HsiW 20% USP	HPW 5% USP	HPW 10% USP	HPW 20% USP	HPMo 5% USP	HPMo 10% USP	HPMo 20% USP	HPW 5% Imp
Removal Ratio (%)	58.97	84.00	53.40	43.40	**90.09**	81.94	**91.46**	48.83	40.00	21.72	86.35
Reaction Rate (10^{-2} min^{-1})	0.952	1.392	0.927	0.750	**1.531**	1.402	**1.538**	0.813	0.660	0.362	1.452
Mineralization Yield (%)	49.30	75.77	70.75	61.38	**86.90**	72.32	47.62	37.15	29.44	16.94	52.15

The bold value represents the most important information in the table.

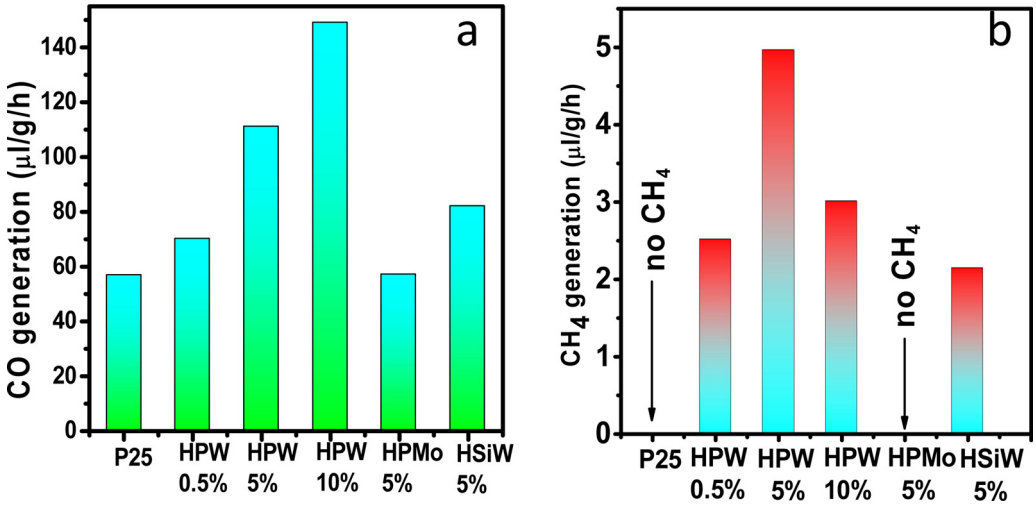

Fig. 7. Photocatalytic production yield of CO and CH_4 over different samples after reaction for 5.5 h.

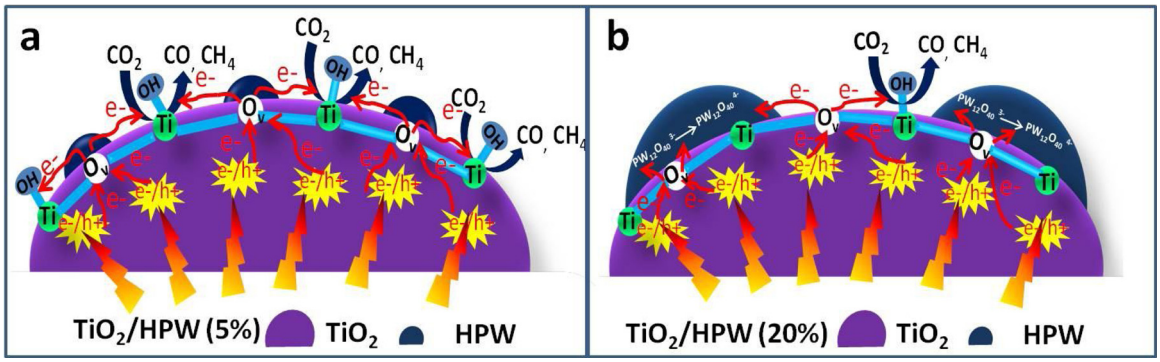

Scheme 2. Photocatalytic reduction of CO_2 over two TiO_2-HPW samples.

it is deduced that oxygen vacancy typed HPW(5%)-TiO_2 exhibits the highest activity in photocatalytic reactions via multielectron transfer. Moreover, note that the redox potential for CO_2/CO and CO_2/CH_4 is more negative than the LUMO level of HSiW (0.06 V), HPW (0.22 V), and HPMo (0.65 V), respectively. Nevertheless, in the case of multi-electron transfer, part of ground state HPW^- could generate multi-electron photoinduced HPW^-*. The redox potential of HPW^-* is more negative than that of HPW [57,58]. In other words, the excited-state HPW^-* has stronger reduction ability than that of ground-state HPW^-. Therefore, it is suggested that the multielectron photoinduced HPW^-* serve as active cites for onset of CO_2 reduction. The mechanism for photocatalytic reduction of CO_2 over HPW-TiO_2 is illustrated in Scheme 2. In this scheme, the difference of activity between HPW(5%)-TiO_2 and HPW(20%)-TiO_2 is also illustrated, which is believed to result from the dispersion of HPW.

3.5. Photochromic phenomena over POM-TiO_2 composite

To further understand the reason for higher activity towards acetaldehyde mineralization and CO_2 reduction over oxygen vacancy typed POM-TiO_2, we irradiated the catalyst at anaerobic condition and monitor photochromic phenomenon over catalyst. When TiO_2 is irradiated under UV light in aerobic atmosphere, the photogenerated electrons tend to transfer to oxygen via single electron transfer. On the contrary, in anaerobic atmosphere, photogenerated electrons are deemed to be either accumulated in TiO_2 or reacted with surface adsorbed substance. Therefore, the photochromic phenomena observed in TiO_2 under irradiation in anaerobic atmosphere is governed by balance rate of electron accumulation and surface reactions [59,60]. As shown in Fig. 8a, after irradiation for 30 min, the color of oxygen vacancy typed TiO_2 turns blue, which is in agreement with results in previous studies [59]. Differently, oxygen vacancy typed HPW(5%)-TiO_2 hardly shows color change no matter long-time irradiation for 30 min. In principle, if the electron accumulation is dominate, Ti^{4+} can be reduced to Ti^{3+} and the color of TiO_2 catalyst will be changed to blue, as schemed in Fig. 8b, top. Alternatively, if the rate of electron involved surface reaction is equal or even higher than that of electron accumulation, the TiO_2 catalyst could maintain its natural white color. Accordingly, for oxygen vacancy typed TiO_2, the blue color after irradiation in anaerobic atmosphere means that the oxygen vacancy tends to trap photogenerated electrons but are difficult to transfer to TiO_2 surface because of the lack of electron acceptors on the TiO_2 surface. On the contrary, for oxygen vacancy typed HPW(5%)-TiO_2, no change of color after irradiation in anaerobic atmosphere means that trapped photogenerated electrons around the oxygen vacancy could quickly transfer to HPW on the surface and react with surface adsorbed substance, as schemed in Fig. 8b, middle. In combination with above comprehensive analysis, it is believed that the constant white color of oxygen vacancy typed HPW-TiO_2 originates from fascinating energy level match between oxygen vacancy typed TiO_2 and HPW, which promote not only separation of charge carrier but also surface reaction of electron with acetic acid or CO_2. In the case of oxygen vacancy typed HPW(10%)-TiO_2, it is noted that they appear a blue color, indicating more accumulation of electrons in TiO_2 and thereafter less consumption of electrons by surface reaction than that of oxygen vacancy typed HPW (5%)-TiO_2, as schemed in Fig. 8b, bottom. On recalling aforementioned comprehensive analysis, the back transfer of electron from HPW to TiO_2 can not be neglected, it is thought that the back transfer of electron

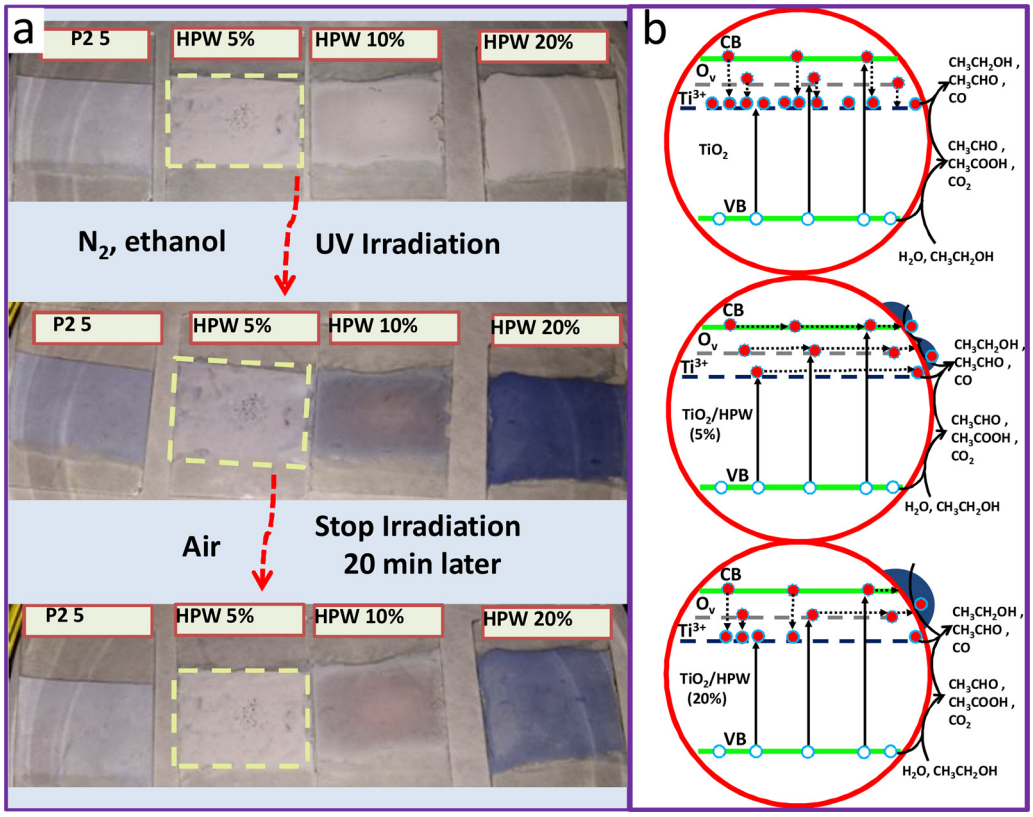

Fig. 8. Photochromic phenomena over different samples when irradiated in nitrogen and ethanol atmosphere for 30 min, and then stop irradiation and expose in air for 20 min. (For interpretation of the references to colour in the text, the reader is referred to the web version of this article.)

hampers the flow of electrons located around oxygen vacancy to surface adsorbed substance via HPW medium, and therefore results in Ti^{3+} formation. By comparing photochromic phenomena between different samples, it is safe to conclude that energy level match between oxygen vacancy typed TiO_2 and POM is beneficial to not only charge separation but also thereafter surface reaction.

4. Conclusion

In this work, an ultraspray pyrolysis technique is employed to assemble TiO_2-POM microspheres. It is found that oxygen vacancy is introduced into TiO_2, and interestingly, such oxygen vacancy induce better match of energy level between defective TiO_2 and Keggin POM, which is beneficial to charge separation and hence multielectron accumulation. The presence of oxygen vacancy is adverse to charge separation in plain TiO_2, and whereas oxygen vacancy type TiO_2-POM become a better candidate for multielectron involved reaction due to proper energy level match induced multielectron transfer. In particular, HPW(5 wt%)-TiO_2 exhibits the highest mineralization yield and CH_4 selectivity among all samples, benefiting from best energy level match and strong interaction between TiO_2 and HPW component. This simple but effective means on the basis of energy level match and coctalyst can be extended to apply doped semiconductor-POM system for highly active photocatalyst.

Acknowledgements

This work was supported by the Natural Science Foundation of China (Grant Nos. 51072032, 51372036 and 51102001), the Key Project of Chinese Ministry of Education (No 113020A), the 111 project (No. B13013), China Postdoctoral Science Foundation (2014M551156), Jilin Province Science and Technology Development Plan (20160520170JH) and Jilin Provincial Education Department Project (No. 52, 2016).

Appendix A. Supplementary data

Supplementary material related to this article can be found, in the online version, at doi:https://doi.org/10.1016/j.apcatb.2018.04.015.

References

[1] M.R. Hoffmann, S.T. Martin, W. Choi, D.W. Bahnemann, Chem. Rev. 95 (1995) 69–96.
[2] X. Chen, S.S. Mao, Chem. Rev. 107 (2007) 2891–2959.
[3] A. Fujishima, X. Zhang, D.A. Tryk, Surf. Sci. Rep. 63 (2008) 515–582.
[4] L. Hammarstrom, Acc. Chem. Res. 48 (2015) 840–850.
[5] H.H. Mohamed, C.B. Mendive, R. Dillert, D.W. Bahnemann, J. Phys. Chem. A 115 (2011) 2139–2147.
[6] K. Rajeshwar, C. Janaky, W. Lin, D.A. Roberts, W. Wampler, J. Phys. Chem. Lett. 4 (2013) 3468–3478.
[7] H. Park, H. Kim, G. Moon, W. Choi, Energy Environ. Sci. 9 (2016) 411–433.
[8] M. Nolan, A. Iwaszuk, A.K. Lucid, J.J. Carey, M. Fronzi, Adv. Mater. 28 (2016) 5425–5446.
[9] C. Wang, X. Zhang, Y. Liu, Appl. Surf. Sci. 358 (2015) 28–45.
[10] J. Yang, D. Wang, H. Han, C. Li, Acc. Chem. Res. 46 (2013) 1900–1909.
[11] H. Tada, Q. Jin, A. Iwaszuk, M. Nolan, J. Phys. Chem. C 118 (2014) 12077–12086.
[12] R. Abe, H. Takami, N. Murakami, B. Ohtani, J. Am. Chem. Soc. 130 (2008) 7780–7781.
[13] M.V. Dozzi, G.L. Chiarello, M. Pedroni, S. Livrghi, E. Giamello, E. Selli, Appl. Catal. B: Environ. 209 (2017) 417–428.
[14] Y. Lv, Y. Zhu, Y. Zhu, J. Phys. Chem. C 117 (2013) 18520–18528.
[15] X. Bai, L. Wang, R. Zong, Y. Lv, Y. Sun, Y. Zhu, Langmuir 29 (2013) 3097–3105.
[16] D. Liu, Y. Lv, M. Zhang, Y. Liu, Y. Zhu, R. Zong, Y. Zhu, J. Mater. Chem. A 2 (2014) 15377–15388.
[17] Z. Wang, C. Yang, T. Lin, H. Yin, P. Chen, D. Wan, F. Xu, F. Huang, J. Lin, X. Xie, M. Jiang, Energy Environ. Sci. 6 (2013) 3007–3014.
[18] J. Wang, Z. Wang, B. Huang, Y. Ma, Y. Liu, X. Qin, X. Zhang, Y. Dai, ACS Appl. Mater. Interfaces 4 (2012) 4024–4030.
[19] M. Xing, J. Zhang, F. Chen, B. Tian, Chem. Commun. 47 (2011) 4947–4949.
[20] Z. Lin, A. Orlov, R.M. Lambert, M.C. Payne, J. Phys. Chem. B 109 (2005) 20948–20952.
[21] M. Miyauchi, H. Irie, M. Liu, X. Qiu, H. Yu, K. Sunada, K. Hoshimoto, J. Phys. Chem.

Lett. 7 (2016) 75–84.
[22] R. Kumar, S. Govindarajan, R.K.S.K. Janardhana, T.N. Rao, S.V. Joshi, S. Anandan, ACS Appl. Mater. Interfaces 8 (2016) 27642–27653.
[23] M. Liu, X. Qiu, M. Miyauchi, K. Hashimoto, J. Am. Chem. Soc. 135 (2013) 10064–10072.
[24] M.G. Mendez-Medrano, E. Kowalska, A. Lehoux, A. Herissan, B. Ohtani, D. Bahena, V. Briois, C. Colbeau-Justin, J.L. Rodriguez-lopez, H. Remita, J. Phys. Chem. C 120 (2016) 5143–5154.
[25] H. Yu, H. Irie, K. Hashimoto, J. Am. Chem. Soc. 132 (2010) 6898–6899.
[26] S. Kim, H. Park, W. Choi, J. Phys. Chem. B 108 (2004) 6402–6411.
[27] P. Kormali, A. Troupis, T. Triantis, A. Hiskia, E. Papaconstantinou, Catal. Today 124 (2007) 149–155.
[28] H. Park, W. Choi, J. Phys. Chem. B 107 (2003) 3885–3890.
[29] M. Yoon, J.A. Chang, Y. Kim, J.R. Choi, K. Kim, S.J. Lee, J. Phys. Chem. B 105 (2001) 2539–2545.
[30] Y. Guo, C. Hu, J. Mol. Catal. A 262 (2007) 136–148.
[31] K. Lv, Y. Xu, J. Phys. Chem. B 110 (2006) 6204–6212.
[32] Y. Li, S. Ouyang, H. Xu, X. Wang, Y. Bi, Y. Zhang, J. Ye, J. Am. Chem. Soc. 138 (2016) 13289–13297.
[33] L. Peng, T. Xie, Y. Lu, H. Fan, D. Wang, Phys. Chem. Chem. Phys. 12 (2010) 8033–8041.
[34] H. Fan, H. Li, B. Liu, Y. Lu, T. Xie, D. Wang, ACS Appl. Mater. Interfaces. 4 (2012) 4853–4857.
[35] L. Zhang, S. Li, B. Liu, D. Wang, T. Xie, ACS Catal. 4 (2014) 3724–3729.
[36] H. Fan, T. Jiang, H. Li, D. Wang, L. Wang, J. Zhai, D. He, P. Wang, T. Xie, J. Phys. Chem. C 116 (2012) 2425–2430.
[37] J.H. Bang, R.J. Helmich, K.S. Suslick, Adv. Mater. 20 (2008) 2599–2603.
[38] S.S. Dunkle, R.J. Helmich, K.S. Suslick, J. Phys. Chem. C 113 (2009) 11980–11983.
[39] L. Li, C.K. Tsung, Z. Yang, G.D. Stucky, L.D. Sun, J.F. Wang, C.H. Yan, Adv. Mater. 20 (2008) 903–908.
[40] S.H. Choi, Y.N. Ko, J.K. Lee, Y.C. Kang, Adv. Funct. Mater. 25 (2015) 1780–1788.
[41] L. Kong, X. Zhang, C. Wang, F. Wan, L. Li, Chin. J. Catal. 38 (2017) 2120–2131.
[42] L. Kong, C. Wang, H. Zheng, X. Zhang, Y. Liu, J. Phys. Chem. C 119 (2015) 16623–16632.
[43] H. Zheng, C. Wang, X. Zhang, L. Kong, Y. Li, Y. Liu, Y. Liu, New J. Chem. 40 (2016) 3225–3232.
[44] J. Li, X. Sang, W. Chen, C. Qin, S. Wang, Z. Su, E. Wang, Eur. J. Inorg. Chem. 2013 (2013) 1951–1959.
[45] J.A. Rengifo-Herrera, M. Blanco, J. Wist, P. Florian, L.R. Pizzio, Appl. Catal. B: Environ. 189 (2016) 99–109.
[46] L. Li, Q. Wu, Y. Guo, C. Hu, Microporous Mesoporous Mater. 87 (2005) 1–9.
[47] M. Misono, Catal. Rev. Sci. Eng. 29 (1987) 269–321.
[48] L. Kong, Z. Jiang, C. Wang, F. Wan, Y. Li, L. Wu, J. Zhi, X. Zhang, S. Chen, Y. Liu, ACS Appl. Mater. Interfaces 7 (2015) 7752–7758.
[49] J.M. Coronado, J. Soria, Catal. Today 123 (2007) 37–41.
[50] E. Carter, A.F. Carley, D.M. Murphy, J. Phys. Chem. C 111 (2007) 10630–10638.
[51] T. Jiang, T. Xie, Y. Zhang, L. Chen, L. Peng, H. Li, D. Wang, Phys. Chem. Chem. Phys. 12 (2012) 15746–15781.
[52] L. Jing, S. Li, S. Song, L. Xue, H. Fu, Solar Energy Mater. Solar Cells 92 (2008) 1030–1036.
[53] X. Zhang, L. Zhang, T. Xie, D. Wang, J. Phys. Chem. C 113 (2009) 7371–7378.
[54] K. Pruethiarenun, A. Nakajima, J. Jpn. Soc. Colour Mater. 87 (2014) 227–234.
[55] A. Hiskia, A. Mylonas, E. Papaconstantinou, Chem. Soc. Rev. 30 (2001) 62–69.
[56] C. Chen, P. Lei, H. Ji, W. Ma, J. Zhao, H. Hidaka, N. Serpone, Environ. Sci. Technol. 38 (2004) 329–337.
[57] N. Fu, Z. Jin, Y. Wu, G. Lu, D. Li, J. Phys. Chem. C 115 (2011) 8586–8593.
[58] S. Yanagida, A. Nakajima, T. Sasaki, Y. Kameshima, K. Okada, Chem. Mater. 20 (2008) 3757–3764.
[59] J. Yang, X. Zhang, H. Liu, C. Wang, S. Liu, P. Sun, L. Wang, Y. Liu, Catal. Today 201 (2013) 195–202.
[60] T. Tatsuma, S. Saitoh, P. Ngaotrakanwiwat, Y. Ohko, A. Fujishima, Langmuir 18 (2002) 7777–7779.